ELSEVIER

Materials Science and Engineering A360 (2003) 214–219

MATERIALS SCIENCE & ENGINEERING A

www.elsevier.com/locate/msea

Microscopic modelling of simultaneous two-phase precipitation: application to carbide precipitation in low-carbon steels

Michel Perez [a,*], Alexis Deschamps [b]

[a] Groupe d'Étude de Métallurgie Physique et de Physique des Matéraux, UMR CNRS 5510, INSA Lyon, 69621 Villeurbanne Cedex, France
[b] Laboratoire de Thermodynamique et de Physico-Chimie Métallurgique, UMR CNRS 5614, BP 75, 38 402 Saint Martin d'Hères Cedex, France

Received 20 November 2002; received in revised form 19 May 2003

Abstract

A thermodynamically-based precipitation model, employing the classical nucleation and growth theories, has been adapted to deal with simultaneous precipitation of metastable and stable phases. This model gives an estimation of the precipitation kinetics (time evolution of radius and density of precipitates for both phases, as well as the evolution of solute fraction) in a wide range of temperature. Results were successfully compared with an experimental isothermal precipitation diagram (Time–Temperature-Transformation, TTT) from the literature for the precipitation of ϵ carbide and Fe_3C in low-carbon steels.

Keywords: Precipitation; Modelling; Low carbon steel

1. Introduction

Many metallic alloys for structural applications gain their mechanical properties through the small-scale precipitation of a second phase [1,2]. The phase transformation leading to an optimum distribution of hardening precipitates from a supersaturated solid solution (SSS) is often complex, involving a sequence of metastable phases, which compensate a higher Gibbs energy by coherent or semi-coherent interfaces with the metallic matrix. Important industrial examples of such precipitation sequences include SSS $\rightarrow \epsilon \rightarrow Fe_3C$ in iron–carbon alloys [3], SSS $\rightarrow$ BCC copper $\rightarrow$ 9R copper $\rightarrow$ FCC copper (ϵ) in iron–copper alloys [4], SSS $\rightarrow$ GP zones $\rightarrow \beta'' \rightarrow \beta' \rightarrow \beta$ (Mg_2Si) in Al–Mg–Si alloys [5] and GP zones $\rightarrow \eta' \rightarrow \eta$ ($MgZn_2$) in Al–Zn–Mg alloys [6].

In order to optimise the fabrication process of such materials, much effort has been devoted to model the precipitation kinetics and the relationship between the precipitate microstructure and the resulting mechanical properties. Such models have been developed at different scales depending on the problem to be solved.

At the atomic scale, numerical methods based on statistical physics (Monte Carlo), give a precise description of precipitation (formation of clusters, growth and coarsening of precipitates [7,8]. These methods give a space–time description of precipitation but require precise knowledge of interaction potentials between the different atomic species. Moreover, they are still restricted to the first stages of precipitation. These methods have been successfully used in the description in simple systems such as the precipitation of the coherent BCC Cu phase in Fe.

At the mesoscopic scale, the phase field method predicts space and time evolution of both the local order parameter and the solute atoms fraction [9]. It gives a description of the entire microstructure including the interface. This method is very efficient in describing order/disorder transformations, but fails to take into account phenomena such as nucleation.

At a microscopic scale, the equations individually established for the three stages of precipitation kinetics (nucleation, growth and coarsening) have been extensively used in integrated precipitation models [9]. These equations can be either combined or numerically solved to give the evolution of the mean precipitation char-

* Corresponding author. Tel.: +33-4-7243-8063; fax: +33-4-7243-8539.
E-mail address: michel.perez@insa.lyon.fr (M. Perez).

0921-5093/03/$ - see front matter
doi:10.1016/S0921-5093(03)00431-3

acteristics (size and volume fraction) [10,11], or used as tools to calculate the evolution of a complete size distribution [12]. The versatility and small computing time associated with these models has lead to the successful description of relatively complicated situations, such as competitive precipitation at different nucleation sites (e.g. matrix and dislocations) [10], or non-isothermal precipitation in ternary systems (application to Al–Mg–Si alloys [13]).

However, in all cases the description of the precipitation kinetics was limited to one single phase (which can be metastable or stable). The precipitation kinetics in a regime where a precipitation sequence involving several phases is present has received very little attention. At best, the effect of the presence of a metastable phase on the precipitation of the stable phase has been considered as a nucleation efficiency parameter [11]. The interaction of different types of precipitate in a competitive situation (metastable vs. stable) can be of three types:

1. in situ transformation of the metastable phase into the stable phase (e.g. the Fe–Cu system) [14];
2. heterogeneous nucleation of the stable phase on the metastable precipitates (e.g. the Al–Zn–Mg system) [15];
3. independent nucleation of both phases in the matrix (e.g. the Fe–C [16] or the Al–Mg–Si system).

The purpose of the present paper is to present a description of competitive precipitation of two phases of different stability, in the simplest of these three situations, namely (iii), where the two precipitate families are simply related by the common solid solution. For this purpose, the precipitation model of Deschamps and Bréchet [10], based on the classical nucleation, growth and coarsening theories, will be adapted to the two-phases situation. In Section 2, the physical meaning of these equations will be recalled and the coupling between the different phases and the solid solution will be introduced. Results of this approach are presented in Section 3 and are applied to the Fe–C system presenting two stages of precipitation (metastable ϵ-phase and "stable" Fe_3C'). Finally, our results are compared with Time–Temperature-Transformation (TTT) diagrams obtained from electrical conductivity measurements [17].

2. Model

The model for homogeneous precipitation is based on the model by Deschamps and Bréchet [10]. In the original work, two stages for precipitation are considered for the precipitation kinetics: the first involved simultaneously nucleation and growth, and the second involved simultaneously growth and coarsening. A criterion ruling the crossover from one regime to another was introduced. For the sake of simplicity, this paper deals only with the first stage (nucleation and growth), since coarsening is not a necessary ingredient for the prediction of a TTT diagram.

The nucleation of both phases is governed by the driving force Δg for precipitation. This driving force is estimated by assuming an ideal SSS of mole fraction X_C, leading to (see [1] for more details):

$$\Delta g^{\varphi} = -\frac{kT}{v_{at}} S^{\varphi} \quad \text{with}$$
$$S^{\varphi} = \left[X_p^{\varphi} \ln\left(\frac{X_C}{X_{eq}^{\varphi}}\right) + (1 - X_p^{\varphi}) \ln\left(\frac{1 - X_C}{1 - X_{eq}^{\varphi}}\right)\right], \tag{1}$$

where the superscript φ stands for the metastable (m) or the stable (s) phase, v_{at} is the atomic volume (considered as constant for all species), S^{φ} is a thermodynamical function giving the driving force for nucleation (based on the hypothesis of a diluted and regular solid solution), X_{eq}^{φ}, the equilibrium solute mole fraction (with phase φ) in the matrix, X_p^{φ} the carbon mole fraction in the precipitate, and X_C the current solute mole fraction of the matrix.

The nucleation rate is calculated via the classical Becker–Döring theory, modified by Zeldovich, taking into account the free energy reduction due to phase transformation (Δg) and the free energy increase due to the creation of an interface between both phases. This approach gives the nucleation rate as the derivative of the precipitate density N^{φ} of each phase [1]:

$$\frac{dN^{\varphi}}{dt} = N_0 Z \beta^{*\varphi} \exp\left(-\frac{\Delta G^{*\varphi}}{kT}\right) \exp\left(-\frac{\tau^{\varphi}}{t}\right). \tag{2}$$

N_0 is the number of nucleation sites per unit volume ($\approx 1/v_{at} = 2/a^3$ for a bcc structure with lattice parameter a), Z is the Zeldovich factor ($\approx 1/20$), τ^{φ} is the incubation time. The other parameters of equation (2) are expressed as follows [1]:

$$\beta^{*\varphi} = \frac{4\pi R^{*\varphi^2} D X_{X_{C_0}}}{a^4}, \quad \text{with} R^{*\varphi} = \frac{R_0^{\varphi}}{S^{\varphi}} \quad \text{and}$$
$$R_0^{\varphi} = \frac{2\gamma^{\varphi} v_{at}}{kT}, \tag{3}$$

$$\Delta G^{*\varphi} = \frac{16}{3} \pi \frac{\gamma^{\varphi^3}}{\Delta g^{\varphi^2}}, \tag{4}$$

$$\tau^{\varphi} = \frac{1}{2\beta^{*\varphi} Z}, \tag{5}$$

where $R^{*\varphi}$ is the nucleation radius (and also the equilibrium radius), R_0 is a thermodynamical parameter which has the dimension of a length, γ^{φ} is the matrix/precipitate (phase φ) interfacial energy, D is the diffusion coefficient of solute atoms in the matrix, X_{C_0} is the initial solute mole fraction.

The growth of each precipitate phase is described by the steady-state Zener equation, stating that the solute flux is proportional to the gradient of the solute mole fraction. The precipitate size increase during a time increment dt is then calculated as:

$$\frac{dR^{\varphi}}{dt} = \frac{D}{R^{\varphi}} \cdot \frac{X_C - X_{eq}^{\varphi} \exp(R_0^{\varphi}/(X_p^{\varphi} R^{\varphi}))}{X_p^{\varphi} - X_{eq}^{\varphi} \exp(R_0^{\varphi}/(X_p^{\varphi} R^{\varphi}))} + \frac{1}{N^{\varphi}} \cdot \frac{dN^{\varphi}}{dt} \times (\alpha R^{*\varphi} - R^{\varphi}). \quad (6)$$

The first term corresponds to the growth of existing precipitates (including the Gibbs–Thomson effect) and the second term to the appearance of the new nuclei of size $R^{*\varphi}$. The numerical factor $\alpha = 1.05$ [10] results from the fact that new precipitates only grow if their size is slightly larger than the nucleation size. Note that this equation also describes the dissolution kinetics of metastable precipitates once they are destabilised by the precipitation of the stable phase.

Finally, the coupling between stable and metastable phases is made through the solute balance:

$$X_C = \frac{X_{C_0} - (4/3)\pi(X_p^{(m)} N^{(m)} R^{(m)^3} + X_p^{(s)} N^{(s)} R^{(s)^3})}{1 - (4/3)\pi(N^{(m)} R^{(m)^3} + N^{(s)} R^{(s)^3})}. \quad (7)$$

This last equation assumes that both phases nucleate independently. Nucleation of the stable phase eventually destabilises the metastable phase by decreasing the solute mole fraction in the matrix, which was previously in equilibrium with the metastable phase.

3. Results and discussion

This model has been applied to a low carbon steel (carbon mass fraction: 4.6×10^{-4}), in which the precipitation of metastable ϵ ($Fe_{2-4}C$, $X_p^{(m)} = 1/4$) and Fe_3C', $X_p^{(s)} = 1/4$) phases are observed [17]. Although Fe_3C' is not strictly speaking a stable phase, we will call it, for the sake of simplicity, the stable phase in the following. Indeed, Fe_3C', sometimes called dendritic cementite, appears within the grains between 250 and 450 °C, whereas Fe_3C appears at grain boundaries at temperatures above 450 °C. The coefficient of diffusion of carbon is given by:

$$D = D_0 \exp\left(-\frac{Q_D}{RT}\right), \quad (8)$$

with $D_0 = 6.2 \times 10^{-7}$ m^2 s^{-1} and $Q_D = 80$ kJ mol^{-1} [18].

Determining the solubility limit of carbon in ferrite with good precision is not straight-forward. As mentioned in [19], data from the literature is very scattered (for instance, the solubility limits of carbon in equilibrium with cementite at 600 °C varies from 50 to 100 ppm). However, all data can be satisfactorily described by the relation:

$$X_{eq}^{\varphi} = X_{eq_0}^{\varphi} \exp\left(-\frac{Q_p^{\varphi}}{RT}\right). \quad (9)$$

For the metastable ϵ phase, Wells and Butler [3] proposed the following parameters: $X_{eq_0}{}^{(m)} = 0.026$ and $Q_p^{(m)} = 6800$ cal mol^{-1} = 28.4 kJ mol^{-1}. Note that ϵ precipitates are coherent, leading to a large amount of elastic energy stored around the precipitate. This energy has not been mentioned in the nucleation rate equation. However, Wells and Butler's values result from measurements (internal friction) and, thus, incorporate the elastic energy term.

Concerning the stable phase, Zhu [20] gave the solubility limit of carbon, reporting values in accordance with previous results obtained with the thermoelectric power technique [21] (the protocol is detailed in [19,22]), leading to: $X_{eq_0}{}^{(s)} = 0.01$ and $Q_p^{(s)} = 6800$ cal mol^{-1} = 28.4 kJ mol^{-1}.

The initial value of the solute fraction is the key parameter controlling the driving force for nucleation, and thus the nucleation rate. It depends on the carbon content of the considered alloy, but also on the thermal treatment imposed on the sample. In the following, we will consider an annealing treatment at 700 °C prior to the precipitation treatment, followed by a quench. The initial value of the solute fraction is then equal to the solubility limit of carbon in ferrite at 700 °C. This limit has been measured using thermoelectric power [19] leading to $(1.6 \pm 0.2) \times 10^{-4}$ (mass fraction), or $(7.0 \pm 0.1) \times 10^{-4}$ (mole fraction), in accordance with former results of Stanley [23].

The two main parameters of this model are the interfacial energies between the matrix and the precipitates. As nucleation may be heterogeneous, they do not correspond to true interfacial energies but to effective values, taking into account the heterogeneous aspect of nucleation, and also the non-spherical shape of precipitates. A more complex approach taking into account a heterogeneous nucleation site numbers (N_0 , $\neq N_0$) and a more realistic precipitate shape would lead to similar results, adding more adjustable parameters. Indeed, we assume that N_0 and γ^{φ} do not vary with temperature. This hypothesis will be confirmed by the simulation results.

Moreover, it is not trivial to access values for interfacial energies by experimental means and, to our knowledge, no simulation at the atomic scale (ab initio, molecular dynamics or Monte Carlo) predict any value. Therefore, these two parameters have been fitted to an experimental precipitation kinetics (presented later) at one given temperature, leading to reasonable values: $\gamma^{(m)} = 0.147$ J m^{-2} and $\gamma^{(s)} = = 0.174$ J m^{-2}. They are kept constant for all temperatures. Note that the sensitivity of the model to interfacial energies is very

high because they enter in the activation energy for nucleation with an exponent of 3. Indeed, changing the surface energy by about 2% leads to a time shift in the precipitation kinetics of about 50%.

The set of equations previously derived (evolution of R^{φ}: Eq. (2) and evolution of N^{φ}: Eq. (6)) was integrated numerically using a Runge–Kutta algorithm with an adaptive integration stepsize [24]. Unknown variables are (i) the solute mole fraction (X_C), (ii) the radii of stable ($R^{(s)}$) and metastable ($R^{(m)}$) precipitates, and (iii) the density of stable ($N^{(s)}$) and metastable ($N^{(m)}$) precipitates. The initial precipitate density is zero: $N^{(s)}|_0 = N^{(m)}|_0 = 0$. After the first iteration, the precipitate radii are equal to the nucleation radii: $R^{(s)}|_0 = R^{*(s)}$ and $R^{(m)}|_0 = R^{*(m)}$.

Table 1 gives a complete list of all parameters used in the model for a low carbon steel. A simulated precipitation kinetics will be first presented at 200 °C (corresponding to the domain where both metastable and stable phases appear simultaneously): we will discuss the time evolution of precipitates radius and density, and solute fraction. Finally, precipitation kinetics computed in a wide range of temperature will lead to the TTT diagram that will be compared with experimental data in the literature.

Let us start with a simple case where only the precipitation of the stable phase is permitted. Evolution of stable (s) precipitates radii and transformed volume fraction at 200 °C is shown in Fig. 1. After the incubation time, precipitates start to grow until the solute mole fraction reaches its equilibrium value: $R^{(s)} = R^{*(s)}$. At this stage, growth stops. The transformed fraction of the stable phase (corresponding to $4/3\pi R^{(s)^3} N^{(s)}$) exhibits a classical behaviour (sigma curve).

Fig. 2 shows the radius evolution for both phases at 200 °C. After the incubation time (τ^{φ} of equation 2), precipitates of both phases start to grow simultaneously,

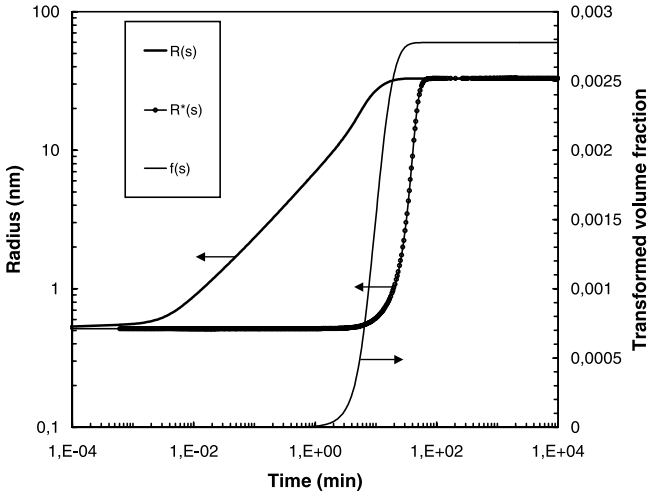

Fig. 1. Evolution of stable (s) precipitate radii and transformed volume fraction at 200 °C, when only the stable phase precipitation is permitted. After the incubation time, precipitates start to grow until the solute mole fraction reaches its equilibrium value: $R^{(s)} = R^{*(s)}$.

following a similar law (note that the number of precipitates of each phase is very different). At a given time, due to the precipitation of the stable phase, the critical radius for dissolution of the metastable phase ($R^{*(m)}$) exceeds the value of their mean radius: this destabilises the metastable phase, which quickly disappears to the benefit of the stable phase, the growth of which is thus accelerated.

Fig. 3 shows the evolution of the density of each precipitate phase at 200 °C. As their nucleation rate is much higher at this temperature, metastable precipitates are dominant in the first stages of the decomposition process: the stable phase becomes dominant only when the metastable phase is destabilised.

The carbon mole fraction evolution in the solid solution at 200 °C is exhibited in Fig. 4. Two well defined stages can be observed: the first one is related to

Table 1
List of the parameters of the model for a low carbon steel

Parameter	Meaning	Value	Source
a	Lattice parameter of bcc iron	2.86^{-10} m	[25]
v_{at}	Atomic volume of bcc iron	$v_{at} = a^3/2$	–
N_0	Number of sites per unit volume	$N_0 = 1/v_{at}$	–
Z	Zeldovich factor	1/20	[26]
$\gamma^{(m)}$	Matrix/metastable phase surface tension	0.147 J m^{-2}	Fit
$\gamma^{(s)}$	Matrix/stable phase surface tension	0.174 J m^{-2}	Fit
D_0	Pre-exp. factor for the diffusion coefficient	6.2×10^{-7} m^2 s^{-1}	[18]
Q_D	Act. energy for the diffusion coefficient	80 kJ mol^{-1}	[18]
X_{C_0}	Initial value of carbon mole fraction	0.0007	[19,23]
$X_{eq_{0(m)}}$	Pre-exp. factor for the solubility limit (m)	0.026	[3]
$X_{eq_{0(s)}}$	Pre-exp. factor for the solubility limit (s)	0.01	[20]
$Q_p^{(m)}$	Act. energy for the solubility limit (m)	28.4 kJ mol^{-1}	[3]
$Q_p^{(s)}$	Act. energy for the solubility limit (s)	28.4 kJ mol^{-1}	[20]
$X_p^{(m)}$	Mole fraction of metastable precipitate	0.25	–
$X_p^{(s)}$	Mole fraction of stable precipitate	0.25	–

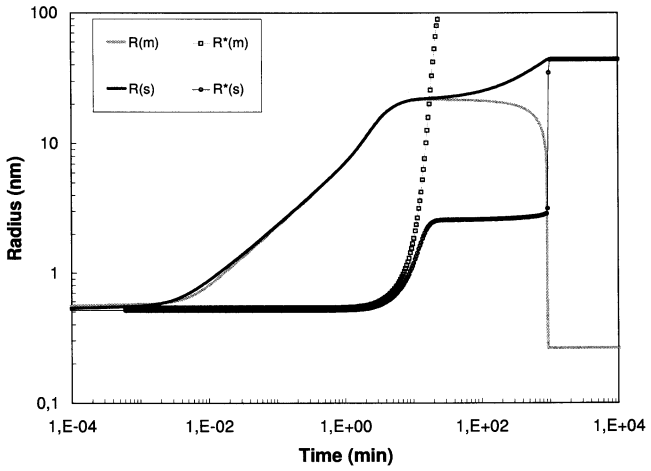

Fig. 2. Evolution of metastable (m) and stable (s) precipitate radii at 200 °C. Precipitates of both phases start to grow simultaneously, following a similar law. At a given time, due to the precipitation of the stable phase, the critical radius for dissolution of the metastable phase ($R^{*(m)}$) exceeds the value of their mean radius: this destabilises the metastable phase, which quickly disappears to the benefit of the stable phase.

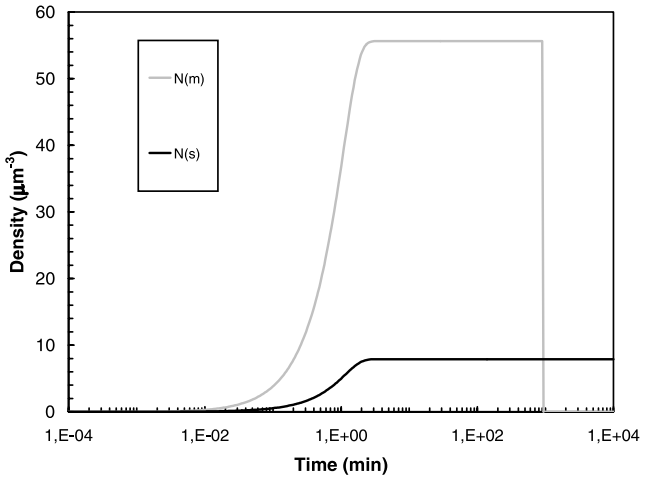

Fig. 3. Number of precipitates per unit volume at 200 °C. The number of metastable phase precipitates is higher until their destabilisation.

the precipitation of ϵ carbides and the second one to the precipitation of cementite.

The total transformed fraction of each phase (corresponding to $4/3\pi R^{\varphi 3} N^{\varphi}$) is represented in Fig. 5. The two stages of the precipitation kinetic appear clearly: the metastable phase nucleates and grows first and is destabilised when the stable phase grows. Note that the metastable phase has a strong effect on the stable phase precipitation kinetics: when the stable phase is alone (see Fig. 1), its precipitation is completed after approximately 10 min at 200 °C, whereas it lasts for approximately 1000 min when both phase precipitate. Indeed, the nucleation rate of the stable phase is much lower after the metastable phase precipitation, that has

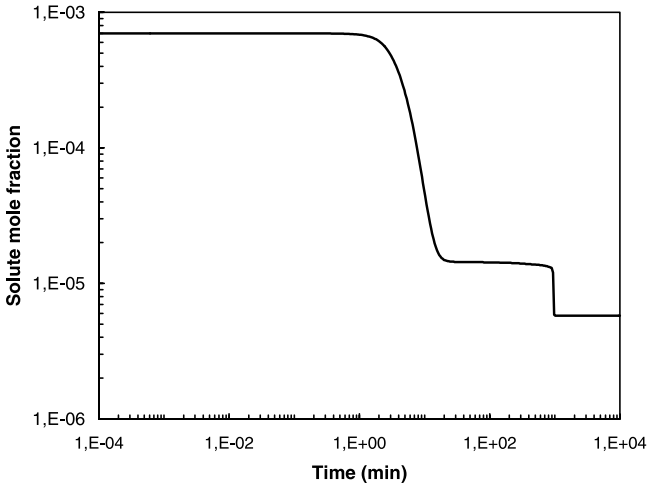

Fig. 4. Concentration of the solid solution at 200 °C: the first step corresponds to the precipitation of the metastable phase and the second step to the precipitation of the stable phase.

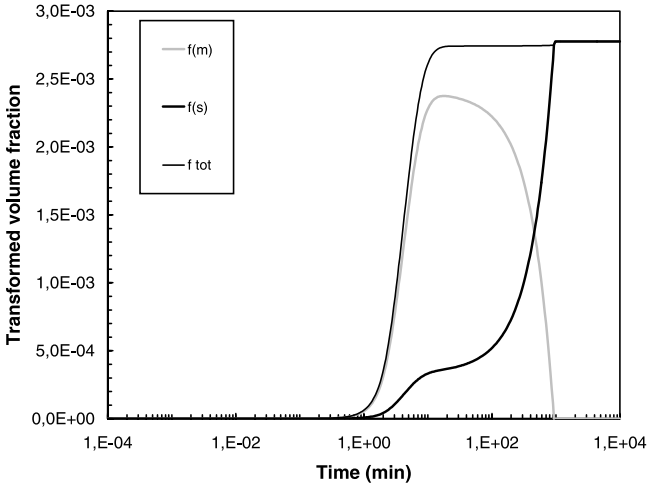

Fig. 5. Transformed fraction vs. time for each phases at 200 °C. The metastable phase is destabilised as the stable phase appears.

"consumed" a large part of solute atoms, leading to a low driving force for nucleation.

The computation presented has been made at temperatures ranging from 100 to 350 °C and the results are presented as a TTT diagram. At each temperature, the time corresponding to a transformed fraction of 60% is considered.

Results of this model have been compared with an iso-thermal precipitation diagram, presented by Abe [17] obtained from resistivity measurements. Abe performed quench-ageing of an aluminium-killed low-carbon steel, which was preliminarily austenitised for 2 h at 920 °C, slowly cooled to room temperature, cold rolled to 75% reduction, held at 700 °C for 20 min and quenched in iced water. The initial carbon fraction in the solid solution is then given by the solubility limit of carbon in ferrite at 700 °C as considered previously. Fig. 6

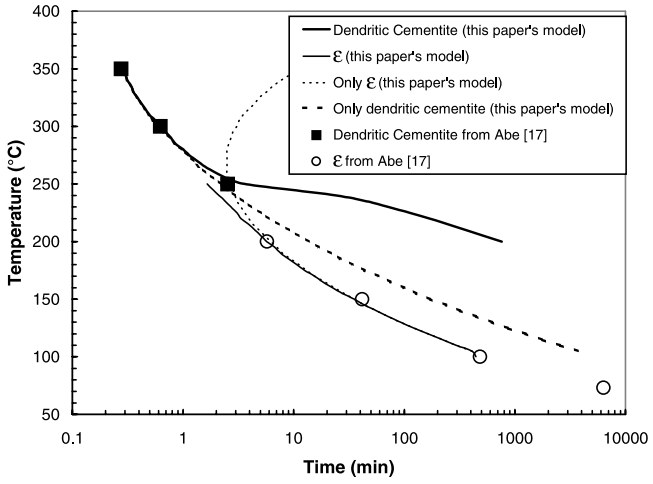

Fig. 6. Comparison between experimental TTT diagram (60% transformed) from resistivity measurements on a low carbon steel and the diagram predicted by the present model. Both diagrams are in very good accordance. The dotted curves show the behaviour of the individual phases.

compares experimental and simulated TTT, or precipitation diagrams. A very good agreement is observed for the two carbides over the whole range of temperatures. As mentioned previously, the metastable phase precipitation has a strong effect on the precipitation sequence kinetics: its appearance leads to longer precipitation time for the stable phase.

4. Conclusion

The microscopic model presented in this paper describes nucleation and growth stages for simultaneous precipitation of metastable and stable phases. It is based on simple assumptions: (1) the estimation of the driving force for precipitation is based on an ideal solution hypothesis; (2) the nucleation rates follow the Becker–Doring theory; (3) both phases nucleate independently; (4) each phase exhibits spherical precipitates, and only the mean radius is considered; (5) coarsening is not included; (6) growth of precipitates (and their dissolution) follows the Zener equation. Under these assumptions, this model describes the competitive precipitation kinetics (in terms of radius, density and solute mole fraction evolution) of a two-phase system, including two precipitates of different stability (called metastable and stable for the sake of simplicity, even if cementite is not truly a stable phase). Results obtained with a quench-ageing low-carbon steel are in good agreement with data from the literature. The model enables to separate the temperature ranges of both phases, as well as the temperature range where the simultaneity of both precipitation phenomena has to be taken into account. In this temperature range, the kinetics of the transition from the metastable to the stable precipitate is also described.

A natural extension of this modelling work will be to include the other characteristic regimes for multi-phase precipitation as described in Section 1. Further development should also include the description of non-isothermal precipitation kinetics, where the transition from metastable to stable phases is particularly relevant. For this purpose, a so-called "class model" describing the evolution of the precipitate size distribution will be used.

Acknowledgements

We are grateful to J. Merlin, Y. Bréchet, A. Vincent and A. Smith for useful discussions.

References

[1] R. Kampmann, R. Wagner, Materials Science and Technology: A Comprehensive Treatment, vol. 5, VCH, Weinheim, 1991, p. 213.
[2] A.J. Ardell, Metall. Trans. A 16A (1985) 2131.
[3] M.G.H. Wells, J.F. Butler, Trans. ASM 59 (1966) 427.
[4] A. Deschamps, M. Militzer, W.J. Poole, ISIJ Int. 41 (2001) 196.
[5] M. Murayama, K. Hono, Acta Mater. 47 (1999) 1537.
[6] H. Löffler, I. Kovacs, J. Lendvai, J. Mater. Sci. 18 (1983) 2215.
[7] F. Soisson, G. Martin, Phys. Rev. B 62 (2000) 203.
[8] T.A. Abinandanan, F. Haider, G. Martin, Acta Mater. 46 (1998) 4243.
[9] H.R. Shercliff, M.F. Ashby, Acta Mater. 38 (1990) 1789.
[10] A. Deschamps, Y. Bréchet, Acta Mater. 47 (1999) 293.
[11] J.C. Werenskiold, A. Deschamps, Y. Bréchet, Mater. Sci. Eng. A293 (2000) 267.
[12] O.R. Myhr, Ø. Grong, Acta Mater. 48 (2000) 1605.
[13] O.R. Myhr, Ø. Grong, S.G. Anderson, Acta Mater. 49 (2001) 65.
[14] P.J. Othen, M.L. Jenkins, G.W. Smith, Philos. Mag. A 70 (1994) 1.
[15] A.K. Mukhopadhyay, Q.B. Yang, S.R. Singh, Acta Metall. 42 (1994) 3083.
[16] A. Brahmi, Ph.D. thesis, INSA, France, 1993, 212.
[17] H. Abe, Scand. J. Met. 13 (1984) 226.
[18] C.J. Smithells, Metals Reference Book, vol. II, Butterworths, London, 1967, p. 683.
[19] J. Merlin, S. Garnier, M. Bouzekri, M. Soler, Revue de Métallurgie, 2002, submitted for publication.
[20] A. Zhu, S.I. Neife, E. Pink, Steel Res. 67 (1996) 507.
[21] J. Merlin, Private communication, 2001.
[22] N. Lavaire, J. Merlin, V. Sardoy, Scripta Mater. 44 (2001) 553.
[23] J.K. Stanley, Trans. AIME 185 (1949) 752.
[24] W.H. Press, S.A. Teukolsky, W.T. Vetterling, B.P. Flannery, Numerical Recipies in C, Cambridge University Press, Cambridge, 1988, p. 994.
[25] D.A. Porter, K.E. Easterling, Phase Transformation in Metals and Alloys, Chapman and Hall, London, 1992, p. 514.
[26] C. Wagner, Z. Electrochem. 65 (1961) 581.